Graphene-Black Phosphorus (G-BP) heterostructure on a silicon platform with enhanced absorption and responsivity over telecom operating wavelength

NEHA[1], CHAKRESH KUMAR[1,*], GHANENDRA KUMAR[2]
[1]University School of Information, Communication & Technology, Guru Gobind Singh Indraprastha University, New Delhi-110 078, India
[2]University School of Automation and Robotics, Guru Gobind Singh Indraprastha University, New Delhi-110 078, India

Black phosphorus (BP) is considered the most promising material for fabricating effective infrared (IR) photodetectors with a broadband photodetection mechanism. It performs exceptional opto-electronic properties. The speed and stability of BP-based photodetector is still a challenge in optical networks. To enhance this property, graphene (G) is mixed with BP to form graphene-black phosphorus (G-BP) heterostructure-based photodetectors. The performance of photodetector is numerically investigated through COMSOL Multiphysics for variable thickness and doping concentration of BP layer. Maximum absorption coefficient of 0.6 is achieved at 60 nm of thickness of BP layer over 900 nm wavelength. The responsivity is less over longer wavelengths. But for optical networks, 1550 nm is considered the telecom operating wavelength. To enhance the efficiency of photodetector over a broad spectrum, thickness and doping concentration of BP layer are modified according to the application. In the proposed work, a successful downlink transmission of 10 Gbps data over a 50 km length of fiber using 1550 nm wavelength in 32-channel high-speed passive optical network (PON) is done with G-BP heterostructure-based photodetector at receiving terminal. The performance of system is investigated for variable thickness and doping level of BP layer, and it is measured in terms of quality factor (Q-factor), bit error rate (BER), jitter, and eye closure obtained from eye diagrams. Simulated results reveal that, at higher thickness (60 nm) of BP layer and moderate doping ($\sim 10^{12}$) concentration of BP layer, maximum Q-factor of 25.3 dB and minimum BER of 1 x 10^{-40} are obtained.

(Received December 29, 2025; accepted June 2, 2026)

Keywords: Graphene, Black phosphorus, Heterostructure, Q-factor, Responsivity, Absorption coefficient

1. Introduction

Two-dimensional (2D) materials have recently attracted significant attention for the fabrication of photodetectors. Due to their extraordinary optoelectronic properties, they have gained popularity among other materials. Tunable band gaps, high gain, high responsivity, high detectivity, compatibility with complementary metal-oxide-semiconductor (CMOS) technology, and low mismatch defects are some key features of these types of materials [1-4]. Graphene is one of the best 2D materials, which gives an ultrafast response. Graphene has high intrinsic carrier mobility, due to which they have been extensively investigated and demonstrated with high speed response. A zero band gap enables fast photo detection in graphene-based photodetectors. It exhibits a broad wave band from ultraviolet (UV) to terahertz (THz), which could not be realised with other photodetectors [5-7]. Despite many merits, there is a certain demerit of low optical absorption. Only 2.3 % of optical signal is absorbed by graphene monolayer. To enhance this, a lot of techniques are employed with the graphene-based photodetectors. Plasmonic nanostructures and waveguide integration are one of them. Through the use of hybrid material, improvement in optical absorption can also be done [8-10]. Black phosphorus is emerging as an ideal candidate for photo detection applications from visible to mid-infrared (MIR) regimes. It possesses a tunable bandgap of approximately 0.3 eV to 2 eV. It has high optical absorption and high responsivity under optical illumination over MIR band. Besides this, it also supports high carrier mobility and ultrafast photo detection [11-13]. To improve the quality of photodetectors, heterostructures have recently been more investigated and demonstrated. Graphene-Black phosphorus (G-BP) heterostructures form a suitable combination of materials for efficient photo detection at telecom (1550 nm) operating wavelengths. Low optical absorption of graphene is resolved by the presence of black phosphorus [14-16]. In photonic integrated chips (PIC), silicon (Si) is a preferred material for integration. Si is compatible with CMOS technology. Hence, most of the heterostructures are formed over Si for advancements in photonics [17-19]. In the proposed work, silicon (Si) is used as a substrate for the G-BP hetero structure. The combination of graphene and black phosphorus enables strong optical absorption, high responsivity, ultra-fast response, high gain, low noise, and high photocurrent [20]. The issue of instability in environmental conditions of black phosphorus is overcome by graphene. Both of the materials compensate for each other's demerits. The built-in electric field in the two-dimensional heterostructure facilitates efficient separation of photo-generated electron–hole pairs at the interface, thereby extending the carrier lifetime and promoting enhanced optical gain and responsivity [21]. In addition to this, the presence of an electric field reduces dark current and noise power present inside the junction. In comparison to other graphene-based hetero structures such as graphene-transition metal dichalcogenides (TMDC) hetero structures, graphene-black phosphorus possesses high carrier mobility and band tunability. Helping in ultrafast and tunable photo detection [22-23]. Black phosphorus's bandgap can be tuned via the number of layers to cover a large band of wavelengths, generally from near-infrared (NIR) to mid-infrared (MIR). Graphene acts as an excellent transport or extraction layer for the photo-generated carriers inside black phosphorus layer [24-26]. The detectivity and signal-to-noise ratio (SNR) of photodetectors are significantly improved by the van der Waals heterostructures of 2D materials. Since they are highly compatible with other materials, lattice mismatch and defects are less likely to be generated [27]. The G-BP hetero structure is considered the most promising hetero structure, offering high responsivity, high detectivity, relatively fast operation, a broad spectral range, and better stability than standalone BP or graphene alone. Becoming well-suited for broadband optical communication receivers, on-chip photonic systems, or multi-band sensing applications [28, 29]. Based on the material chosen in photodetectors, the quality of photo detection is affected in optical networks. With the rapid advancement in the development of van der Waals hetero structure, a lot of research is being conducted in this field. G-BP hetero structure is also one of them. Mixing of materials plays a crucial role in improvement of photo detection. Out of many research works, there is some research work is mentioned here. Nhat Anh Nguyen Phan et al. [30] demonstrated the potential of a metal-insulator-semiconductor (MIS) diode realised with the 2D van der Waals hetero structure consisting of a combination of black phosphorus (BP), thin hexagonal boron nitride (hBN) and graphene (G). Comparative analysis of metal-semiconductor (M-S) with MIS reveals that superior current rectification is achieved in MIS. The performance metrics are evaluated in terms of rectification ratio, ideality factor, and tunnelling behaviour, over a temperature range of 77-300 K. Findings of the work highlighted the potential of MIS diodes in ultrathin nanoelectronics, with a rectification ratio of 3.5×10^2 and an ideality factor of 1.6. Feng Zhou et al. [31] presented an all optical plasmonic modulator working in visible regime based on a graphene/black phosphorus hetero structure. Simulation results confirm that, by adjusting the angle of incident light, this proposed modulator is capable of working in the visible regime with small insertion loss, low consumed energy, highly integrated tunability and large extinction ratio from over 25 dB to 55 dB. In this work main focus is on the effect of variation of angle of incidence on the performance of graphene/black phosphorus hetero structure-based photodetector. Abdelkader Abderrahmane et al. [32] demonstrated black phosphorus-molybdenum diselenide ($BP-MoSe_2$) heterotructure-based photodetector. $BP-MoSe_2$ is realised with gold electrodes, the junction behaves as a p-n junction diode. The ideality factor is found to be 0.36, the effect of Schottky barrier formed between gold and $MoSe_2$ is less in comparison to multi-layered $MoSe_2$ 2D material-based photodetector. Stable photo responsivity and specific detectivity are the main features shown by this type of hetero structure. The photo responsivity and specific detectivity are found to be 1.2 mA/W and 3.14×10^9 $cmHz^{1/2}W^{-1}$ at a laser power of 12.36 μW. Electrical and optoelectronic characterization were carried out using an HP 4155A semiconductor parameter analyzer. Chang Liu [33] has shown that the functionalized-BP/MoS_2 heterojunction can be a multifunctional device with gate-controlled free switching of an optoelectronic detector and memory. Optoelectronic performance of the device is enhanced by gate-modulated photo-gating effect produced by induced artificial traps. The device can achieve an exceptional multi-bit storage (90 states), an ultra-high on/off ratio of 3.5×10^7, an ultra-low dark current of 0.13 pA and a speculative storage period of 10 years in the memory model. Multifunctional properties of the 2D materials using hetero structure are the main focus of this study. Yang Zhou et al. [34] successfully fabricated flexible photodetectors based on group VA mono elemental hetero structures. In this work, BP quantum dots (QDs) with consistent sizes are loaded on bismuth (Bi) nano sheets (NSs) to serve as hole capturers in group VA via a facile sonication approach. With BP QDs, the detector is able to achieve 4.6 $\mu A/cm^2$ photocurrent density at applied 0.8 V bias potential, about 4.2 times that of the Bi NSs. Hao Zhang et al. [35] used density functional theory (DFT) to investigate a three-layer heterostructure composed of graphitic zinc oxide (g-ZnO), black phosphorus and graphene. Low mismatches (below 5%) are found in this type of structure. Due to presence of graphene, thermal fluctuations are reduced and enhanced thermal stability is obtained in comparison to BP/g-ZnO bilayer. The device is analysed through molecular dynamics simulations. Optical properties analysis shows that the G/BP/g-ZnO heterostructure exhibits improved absorption coefficients and red-shifted absorption peaks across a broad spectral range, leading to increased photo detection efficiency. Hence, formation of heterostructures is an essential step in the direction of improvement in photo detection. In optical networks, there are a lot of disturbances or noise signals present in the medium, which distort the original form of signal. At the time of photo detection, signal is again suffered from noise present inside photodetector. So for efficient photo detection, there is a need of effective photodetector. In the proposed work, opto-electronic properties of graphene-black phosphorus (G-BP) heterostructure-based photodetector are investigated through COMSOL Multiphysics. The effect of variable thickness and doping level of BP layer on the photodetection mechanism has been investigated successfully. The proposed photodetector is used in 32-channel high-speed time wavelength divison multiplexing

(TWDM) PON system for transmission of 10 Gbps data over 50 km using 1550 nm wavelength. The performance is measured in terms of Quality factor (Q-factor), bit error rate (BER), jitter and eye closure, obtained from eye diagrams using OptSim. Simulated results reveal that high thickness and moderate doping of BP layer are the essential conditions for achieving maximum Q-factor and minimum BER over longer wavelengths. The whole work is organised into five sections. First section includes introduction, second includes device structure and mathematical modelling, third includes Simulation set up, fourth includes results and discussion, and fifth section includes conclusion.

2. Device structure and mathematical modelling

In this section, a detailed theoretical analysis of an already existing G-BP heterostructure-based photodetector is done. The device is taken with standard dimensions. A 3D view of a G-BP heterostructure-based photodetector is shown in Fig. 1. The device is fabricated with standard dimensions. In this structure, Si is taken as a substrate material with height of 250 nm. To avoid any lattice mismatch defects, a layer of SiO_2 of height 100 nm is fabricated upon Si substrate. The photodetector performs photo detection at a telecom wavelength of 1550 nm. The thickness of graphene is taken as 0.35 nm, while thickness of black phosphorus is taken as 7 nm. This combination of graphene and black phosphorus is considered a heterojunction. Formation of source and drain is done by implanting gold (Au) electrodes on both sides, with a height of 100 nm. In practical manufacturing, G-BP heterostructure is prepared by chemical vapour deposition (CVD) method, and then heterojunction is transferred onto the SiO_2/Si substrate.

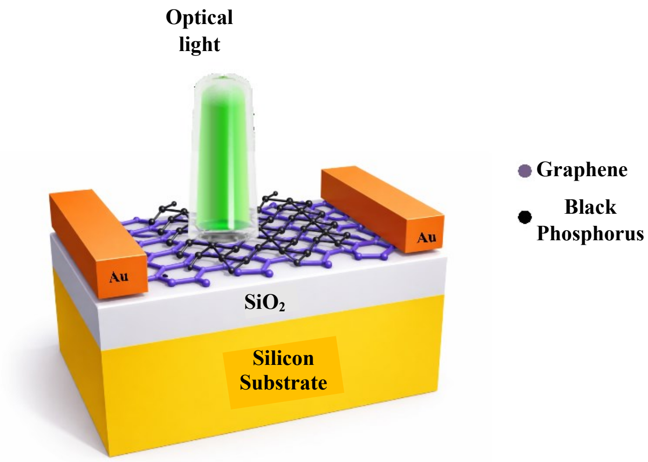

Fig. 1. 3 D view of G-BP heterostructure-based photodetector (colour online)

Black phosphorus is mechanically exfoliated. To define the area of G-BP heterojunction, black phosphorus is selectively removed by ultraviolet (UV) and oxygen plasma etching techniques. Au electrodes are deposited on the surface of graphene through metal deposition method. Since black phosphorus is not stable in air due to chemical degradation, graphene acts as a protective layer for this. Graphene avoids the instability issue of black phosphorus in environmental conditions and ensures long-term stability. In real practice, hexagonal boron nitride (hBN) is used as a protective layer for black phosphorus to avoid any contamination with air. Voltage supply is given between Au electrode fabricated on G-BP heterostructure and Si substrate. Van der Waals structures are highly compatible with other structures, avoiding any type of lattice imperfections. Due to different work potentials of graphene and black phosphorus, a Schottky barrier potential is formed at the junction. Mathematically, it can be represented by equation (1) [36-38].

$$W_B = W_G - \chi_{BP} \tag{1}$$

where W_B is the work potential of black phosphorus, and W_G is the work potential of graphene. χ_{BP} is the electron affinity of black phosphorus. Since black phosphorus is mainly responsible for optical absorption, the doping and thickness of this material affect the performance of detector. The dependence of work potential on doping concentration of black phosphorus can be expressed by equations (2) and (3).

$$W_B^{eff} = W_B - \Delta E_F(N_{bp}) \tag{2}$$

$$\Delta E_F = KT\ln\left(\frac{N_{bp}}{n_i}\right) \tag{3}$$

where N_{bp} is the doping concentration of black phosphorus. W_B^{eff} is the effective barrier height or work potential that depends on BP doping, and n_i is the intrinsic concentration. ΔE_F is the shift in fermi level due to doping. The depletion region width formed between G-BP heterostructure is also affected by doping concentration of black phosphorus. It can be expressed by equation (4). [39-40]

$$W_d = \sqrt{\frac{2\epsilon_{BP}V_{bi}}{qN_{bp}}} \tag{4}$$

where W_d is the depletion region width, ϵ_{BP} is the permittivity, V_{bi} is the barrier potential, and N_{bp} is the doping concentration of black phosphorus. The width is inversely proportional to the doping concentration. With increasing doping, the width is small, resulting in a short transit time for carriers. The electric field intensity increases for smaller depletion widths. There is an inverse relationship between electric field intensity and depletion width. It can be given by equation (5).

$$E_{max} = \frac{2V_{bi}}{W_d} \tag{5}$$

where E_{max} is the maximum electric field that can be formed at the heterojunction. But sometimes excessive doping causes screening at the junction, due to which dark or leakage current increases. It will reduce the magnitude of field. The dark current linearly rises with doping concentration. The dependence of dark current on doping can be given by equation (6).

$$I_{dark} \propto N_{bp} \exp\left(\frac{-W_d}{KT}\right) \quad (6)$$

where I_{dark} is the dark current. At low doping concentration of black phosphorus, about 10^{12} cm^{-3}, there is large depletion width and a strong built-in electric field resulting in very high responsivity and slow response time due to trap-assisted response. At moderate doping levels, approximately 10^{14} cm^{-3}, the electric field is highly balanced, resulting in a reduced recombination rate. Gain is controlled and lower dark current is obtained. In this way doping concentration of black phosphorus plays an important role in deciding photo detection ability of the detector. In addition to this thickness of black phosphorus layer is also an important aspect in the direction of proper photo detection. The variation in thickness affects optical absorption in the layer. The dependence of optical absorption on black phosphorus's thickness is given by equation (7).

$$A = 1 - e^{-\alpha t_{BP}} \quad (7)$$

where α is the optical absorption coefficient, A is the optical absorption and t_{BP} is BP layer thickness. A very thin layer of black phosphorus results in weak absorption. The bandgap of material is dependent on the thickness. Since black phosphorus possess tunable bandgap, it can vary with the thickness. Thin black phosphorus leads to visible/NIR detection, whereas thick black phosphorus leads to IR/mid-IR detection. Carrier transit time is also affected by thickness of the layer. The carrier transit time can be given by equation (8).

$$t_{tr} = \frac{L^2}{\mu V} \quad (8)$$

where L is the carrier transport length, V is the applied bias voltage and t_{tr} is the carrier transit time. Photoconductive gain is obtained in a very controlled manner. It is decided by the responsivity of the photodetector. The responsivity can be given by equation (9).

$$R = \frac{I_{ph}}{P_{opt}} = \eta \frac{q}{h\nu} G \quad (9)$$

where η is the quantum efficiency. I_{ph} is the photocurrent, and P_{opt} is the incident optical power. R is the responsivity, and G is the photoconductive gain. The quality of the signal depends upon the photodetection mechanism performed by photodetector. The optical to electrical conversion is highly affected by the material chosen for photodetector fabrication. The quality factor for the signal received by photodetector depends on the dark current generated inside photodetector. The expression for Q-factor of the received signal can be given by equation (10).

$$Q = \frac{J_1 - J_0}{\sigma_1 - \sigma_0} \quad (10)$$

where $J_1$and J_0 are the mean currents for logic '1' and logic '0' respectively. σ_1 and σ_0 are the noise standard deviations for logic '1' and logic '0'. In this way, G-BP heterostructure-based photodetector performs its operation in a high-speed optical network. Variation in doping concentration and thickness of black phosphorus largely affects the performance of photodetection.

3. Simulation setup

This section presents a detailed analysis of a high-speed 32-channel TWDM/PON system, in which a G-BP heterostructure-based photodetector is utilised at the receiving terminal, specifically on the ONU side. Fig. 2 shows the architecture of proposed system. There are two 16-channel transmitter sections used at OLT side. Each transmitter section consists of pseudo random binary sequence generator (PRBS), a non-return-to-zero (NRZ) modulator drive, continuous wave (CW) laser source, and a Mach-Zehnder modulator (MZM). A binary signal is generated by PRBS and converted to its equivalent electrical form by NRZ modulator driver. CW laser source generates an optical signal, which is used to modulate an electrical signal through MZM. There are two inputs for MZM, one is an electrical signal and other is an optical signal. The same electrical-to-optical conversion occurs through all transmitter sections. Optical signals coming from two 16-channel transmitter sections are combined through an optical combiner. During electro-optic conversion, there are some losses introduced in the signal. To strengthen the signal, a booster is used to give strength to the signal. After boosting a signal, it is transmitted over an optical fiber of length 50 km. An erbium-doped fibre amplifier (EDFA) is used for amplification of the signal. The attenuation of the signal is overcome by the use of this amplifier. To distribute the signal among multiple users, an optical splitter is used. An optical splitter with a splitting ratio of 1 × 2 is used to split signal across two 16-channel receiver sections. There are raised cosine filter, photodetector, and Bessel filter present in the receiver section. Raised cosine filters are used to give optimum gain to the optical signal before photo detection. During transmission of signal, intersymbol interference (ISI) distorts the signal, this distortion can be overcome by the use of a raised cosine filter with an optimum roll-off factor. After this signal is transmitted to G-BP heterostructure-based photodetector. Due to exceptional optoelectronic properties of 2D materials, the obtained electrical signal is of good quality. For further processing electrical signal is transmitted to a Bessel filter. This filter is used to suppress unwanted noise signal present in the electrical signal. Hence, a signal with a good Q-factor is received at the user end. 2D material-based photodetector supports efficient photo detection in high-speed optical networks.

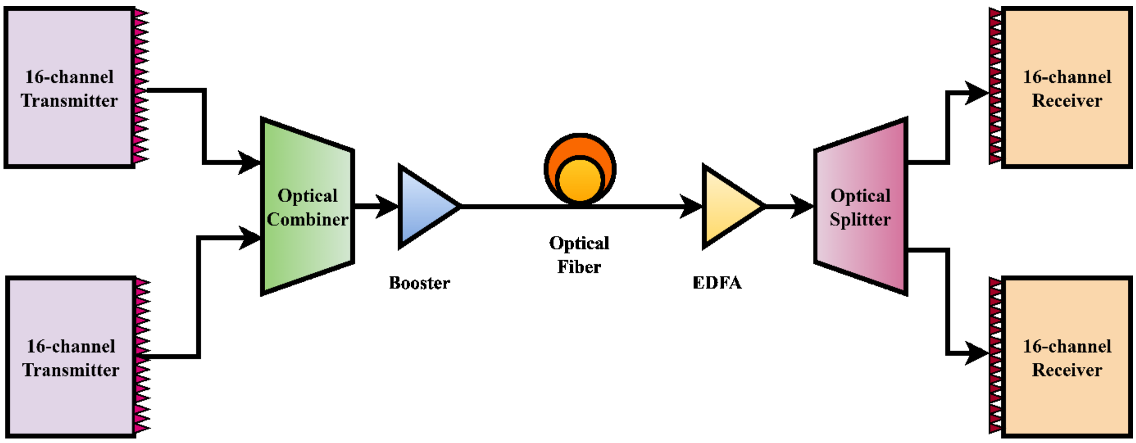

Fig. 2. Block diagram of 32-channel TWDM/PON system using G-BP heterostructure-based photodetector (colour online)

4. Results and discussion

The proposed system is investigated and simulated with G-BP heterostructure-based photodetector at the receiver terminal using OptSim. The optoelectronic properties of G-BP heterostructure-based photodetector are numerically tested through COMSOL Multiphysics. The thickness of BP material plays a crucial role in determining the performance of the photodetector. The performance metrics of photodetectors, such as responsivity, absorption, photocurrent, detectivity, and others, largely depend on the variable doping concentration and thickness of the BP layer. Since absorption is directly related to the thickness of material. Fig. 3(a) shows the relationship between absorption and thickness of BP material. It is observed from the figure that, on increasing thickness of material from 0 to 60 nm, the absorption spectra of BP also increase in the heterostructure. A large number of photons are absorbed in the BP layer, resulting in a high photocurrent. The value of absorption coefficient is about 0.5 or above over a thickness of 60 nm. It is clear from the figure that for lower values of thickness, absorption value is remarkably increased. After 60 nm, the increment in absorption spectra is slow.

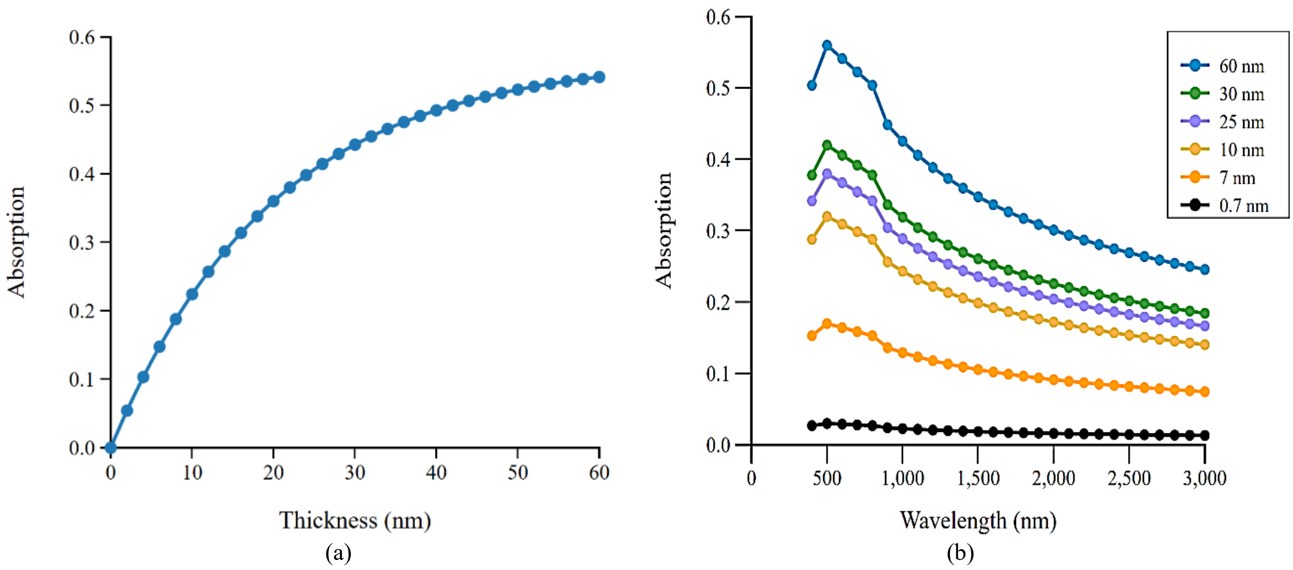

Fig. 3. The variation in absorption spectra of BP in the proposed heterostructure with (a) Variable thickness at a constant wavelength of about 900 nm (b) Variable wavelength as a function of thickness (colour online)

Moreover, to study the thickness-dependent absorption variations, the results are obtained in Fig. 3(b). It is observed from the figure that for longer wavelengths, absorption spectra decrease due to the intrinsic bandgap limitation of BP. At longer wavelengths, the photon excitation energy is reduced, due to which absorption of photons decrease. To enhance this absorption, multiple layers of BP flakes can be used. It is clear from the figure that on increasing thickness from 0 to 60 nm, the absorption is enhanced even at longer wavelengths. The maximum value of absorption is achieved at 60 nm thickness, with a value of about 0.5 above. A thick layer of BP material enhances absorption in G-BP heterostructure-based photodetector. BP acts as an absorber layer, whereas graphene acts as a transport layer, which provides higher carrier mobility to absorbed photons. The incident power of signal decides the photoresponsivity of the detector. The detector is tested for different incident power levels over different wavelengths. Incident optical power has a certain non-linear effect on photoresponsivity of photodetector.

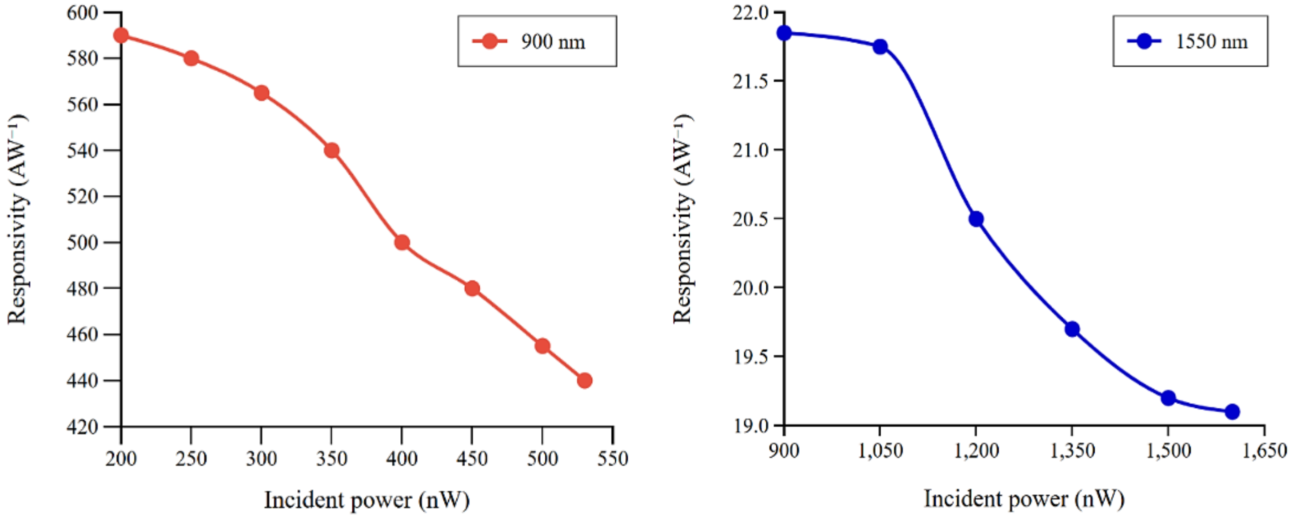

(a) (b)

Fig. 4. The variation of responsivity with incident power over (a) shorter wavelength such as 900 nm (b) longer wavelength such as 1550 nm (colour online)

The dependency of responsivity on incident power for shorter and longer wavelengths is shown in Fig. 4(a) and Fig. 4(b). It is shown in Fig. 4(a) that the absorption is stronger over shorter wavelength 900 nm. There are empty trap states in BP layer, resulting in a strong photo-gating effect. Excessive carriers are generated at low incident power, so that responsivity of photodetector is maximum at this stage. 1μW of signal power is transmitted to the detector, and the responsivity is found to be maximum. As the power increases, the traps become saturated, and excessive carriers recombine with one another. So that photoresponsivity starts to decline. At highest incident power, responsivity is found to be minimum. The variation of responsivity versus incident power for a longer wavelength of 1550 nm is shown in Fig. 4(b). It is observed from the figure that the absorption gets slightly decreased at longer wavelength, due to intrinsic bandgap limitation of BP layer. For low incident power, strong absorption occurs at G-BP junction. High responsivity is obtained for low incident power over 900 nm. In contrast, at high optical power, weaker absorption and reduced carrier separation efficiency result in pronounced responsivity degradation over longer wavelengths. There is another important parameter for which performance of detector is simulated. Doping concentration also plays an important role in affecting photo detection properties of photodetector. Changes in doping concentration of BP layer affect the built-in electric field in G-BP heterostructure. At low doping concentration about $\sim 10^{12}$ the built-in electric field is lower in magnitude at the G-BP junction, resulting in poor carrier separation. Hence, low responsivity is obtained in case of low doping. When doping of BP layer is increased to a moderate level, about $\sim 10^{14}$ the built-in electric field increases, creating efficient charge separation across the junction. Maximum responsivity of about $\sim 6 \times 10^2$ AW^{-1} is achieved at moderate doping. When doping concentration of BP is further increased, the insertion of dark current increases. Dark current reduces the mobility of charge carriers. Due to this, there is a sudden fall in responsivity of detector. Responsivity reaches to its minimum value at high doping concentration of BP layer. The variation of responsivity versus BP doping concentration can be shown in Fig. 5.

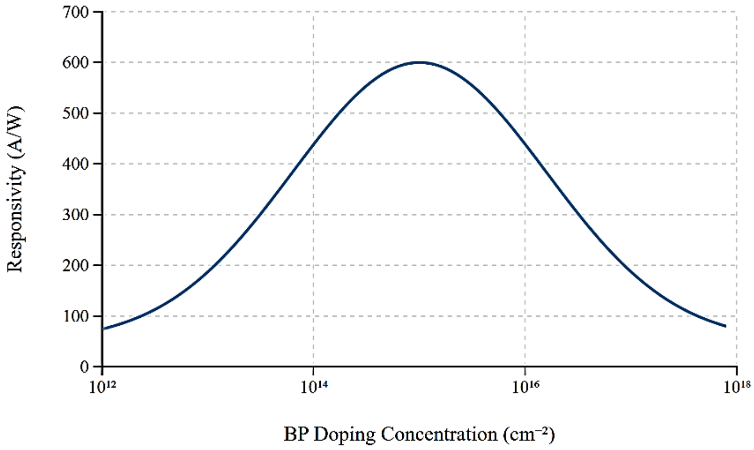

Fig. 5. The variation of responsivity of G-BP heterostructure over variable doping concentration of BP layer

It is observed from the figure that, moderate doping of BP layer gives best results in terms of responsivity. Since responsivity is better at moderate doping, detectivity of photodetector is also improved at this doping level. The effect of doping concentration on built-in-electric field at G-BP junction in a vertical four-layered structure of a photo detector can be shown in Fig. 6(a)-Fig. 6(c).

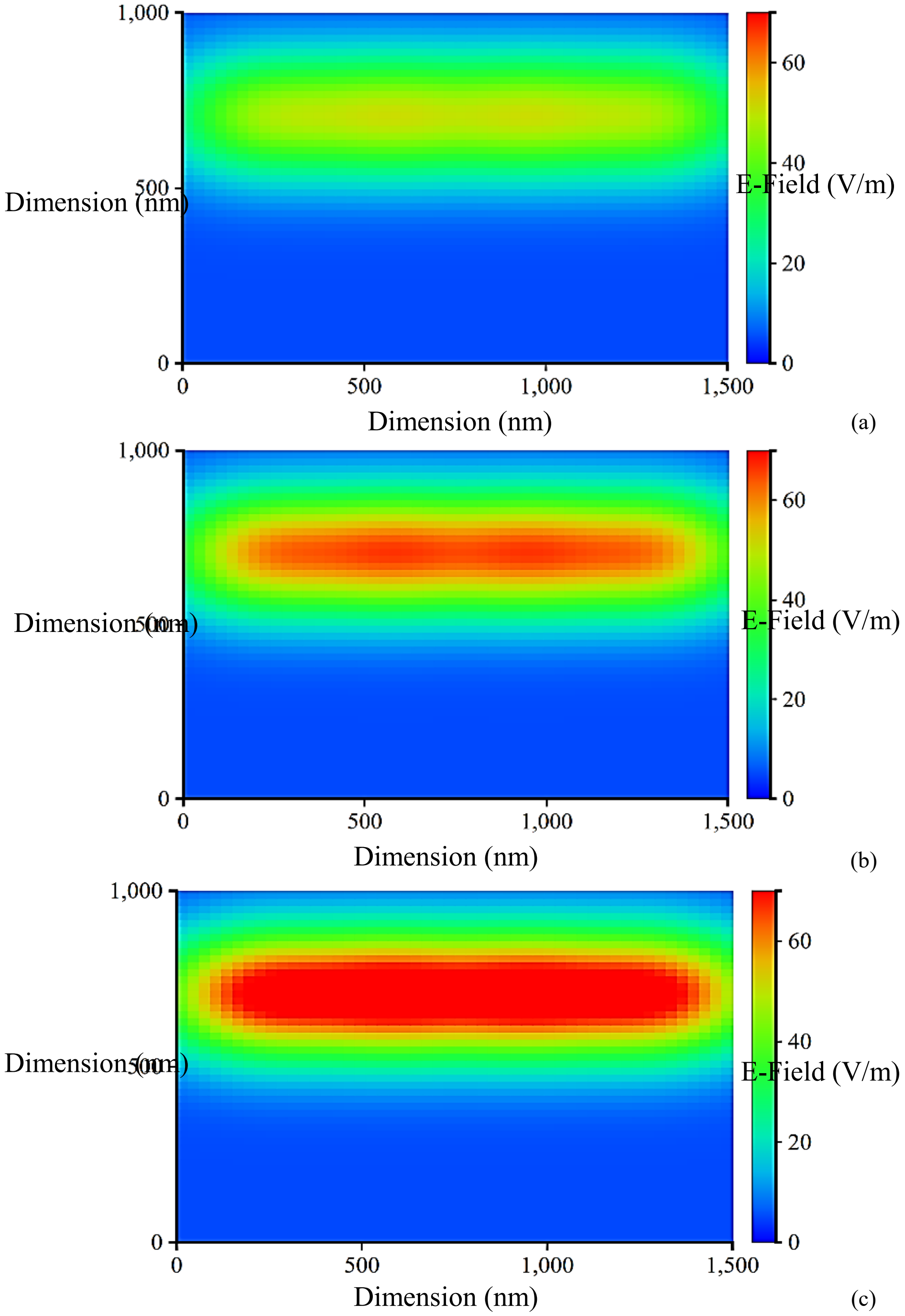

Fig. 6. Variation in built-in-electric field formed in G-BP heterostructure over variable doping concentration of BP layer (a) Low Doping (b) Moderate Doping (c) High Doping (colour online)

Fig. 6(a) shows a weaker electric field distribution in BP layer, because of low doping concentration. External quantum efficiency also gets reduced at this doping level. For improvement in efficiency, the doping concentration of BP layer is increased to a moderate level. Fig. 6(b) shows electric field distribution across the junction at a moderate doping level. It is observed in the figure that, with increasing doping, the carrier density increases with high mobility. The charge carrier separation increases, resulting in strong electric field formation across the junction. Fig. 6(c) shows the electric field distribution at a high doping concentration of BP layer. When the doping concentration is high, the electric field is at its weakest. High doping introduces dark current in the device, which reduces carrier mobility. Responsivity of photodetector also reduces with high doping concentration of BP layer. After numerical simulation of opto-electric properties of G-BP heterostructure-based photodetector. For further analysis, it is implemented in high speed 32-channel passive optical network system to improve signal quality received at ONU side.

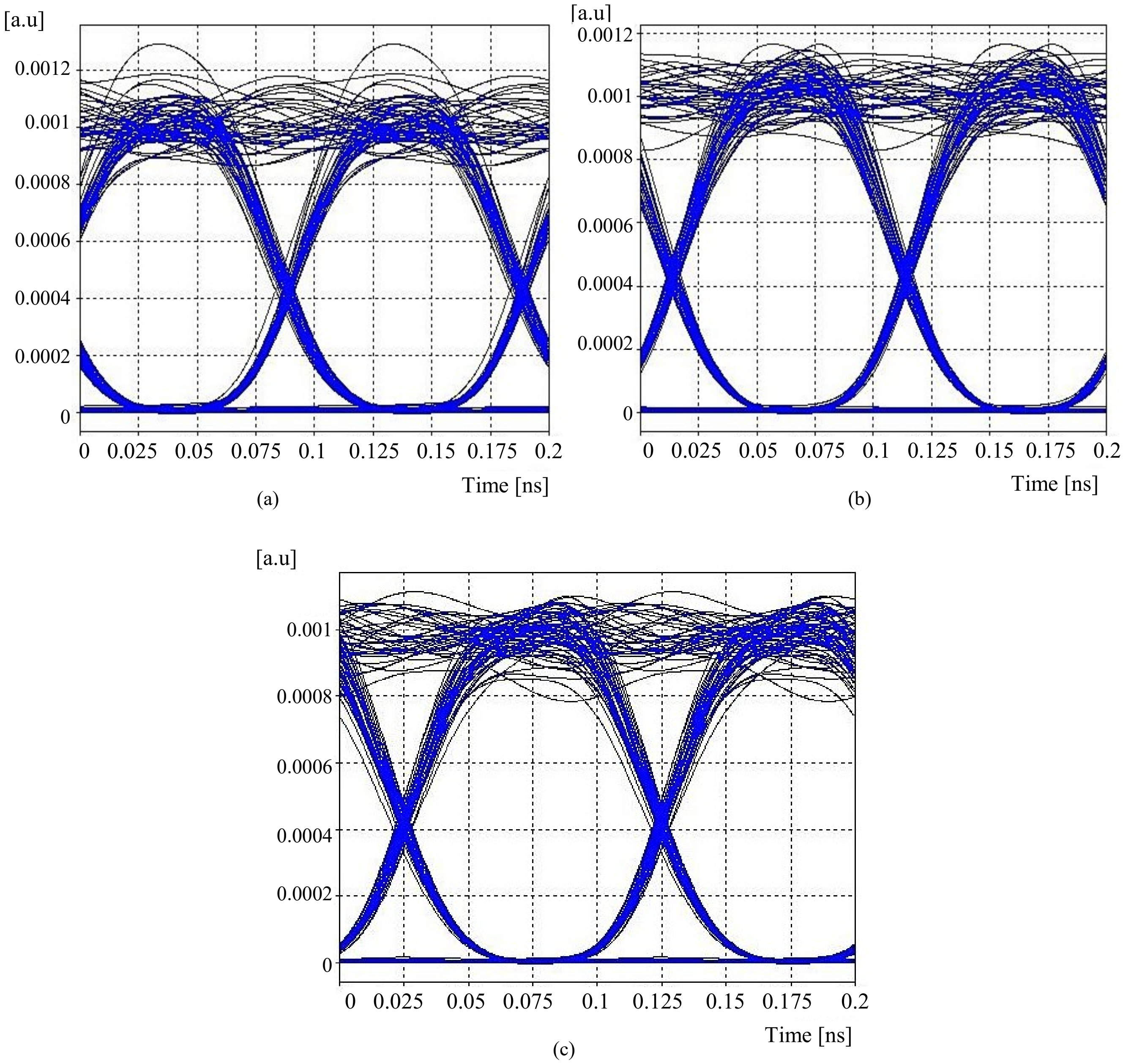

Fig. 7. Eye diagrams obtained for 32-channel TWDM/PON system using G-BP heterostructure-based photodetector over 50 km for variable thickness (a) 10 nm (b) 25 nm (c) 60 nm (colour online)

Fig. 7(a)-7(c) shows the eye diagrams obtained for a 32-channel PON system operating at 1550 nm using a G-BP heterostructure-based photodetector at the receiving terminal for varying thicknesses of the BP layer: 10 nm, 25 nm, and 60 nm in the detector. Fig. 7(a) shows the eye diagram obtained for a 10 nm thickness of BP layer in G-BP heterostructure junction. At a lower thickness, the quality of eye diagram is not good, and the absorption of photons is less. Due to this, the Q-factor of signal is lower in magnitude. 22.9 is the Q-factor, and 1×10^{-32} is the BER achieved by the system over this thickness of BP layer. To see the effect of thickness, the system is simulated for a variable thickness of BP layer. The eye diagram obtained for a 32-channel system using a 1550 nm wavelength for a 25 nm thickness of BP layer is shown in Fig. 7(b). It is observed from the figure that the quality of signal is improved in this case. The absorption of photons increases, which results in high photocurrent or high responsivity. 23 is the Q-factor, and 1×10^{-34} is the BER are achieved by the system over this thickness. The quality of eye diagram is good in comparison to the diagram obtained over a lower thickness. Fig. 7(c) shows the eye diagram obtained for a 32-channel PON system using 1550 nm for a 60 nm thickness. The quality of the received signal is much improved over this thickness. The eye diagram is clear and wide. Maximum Q-factor is achieved over this thickness. 25.3 is the Q-factor and 1×10^{-40} is the BER, obtained in the system over 60 nm. Results reveal that with increasing thickness of BP layer, the quality of signal is affected. For better quality of signal large thickness is preferred. 60 nm gives best results in terms of maximum Q-factor, which is 25.3 dB, with minimum BER.

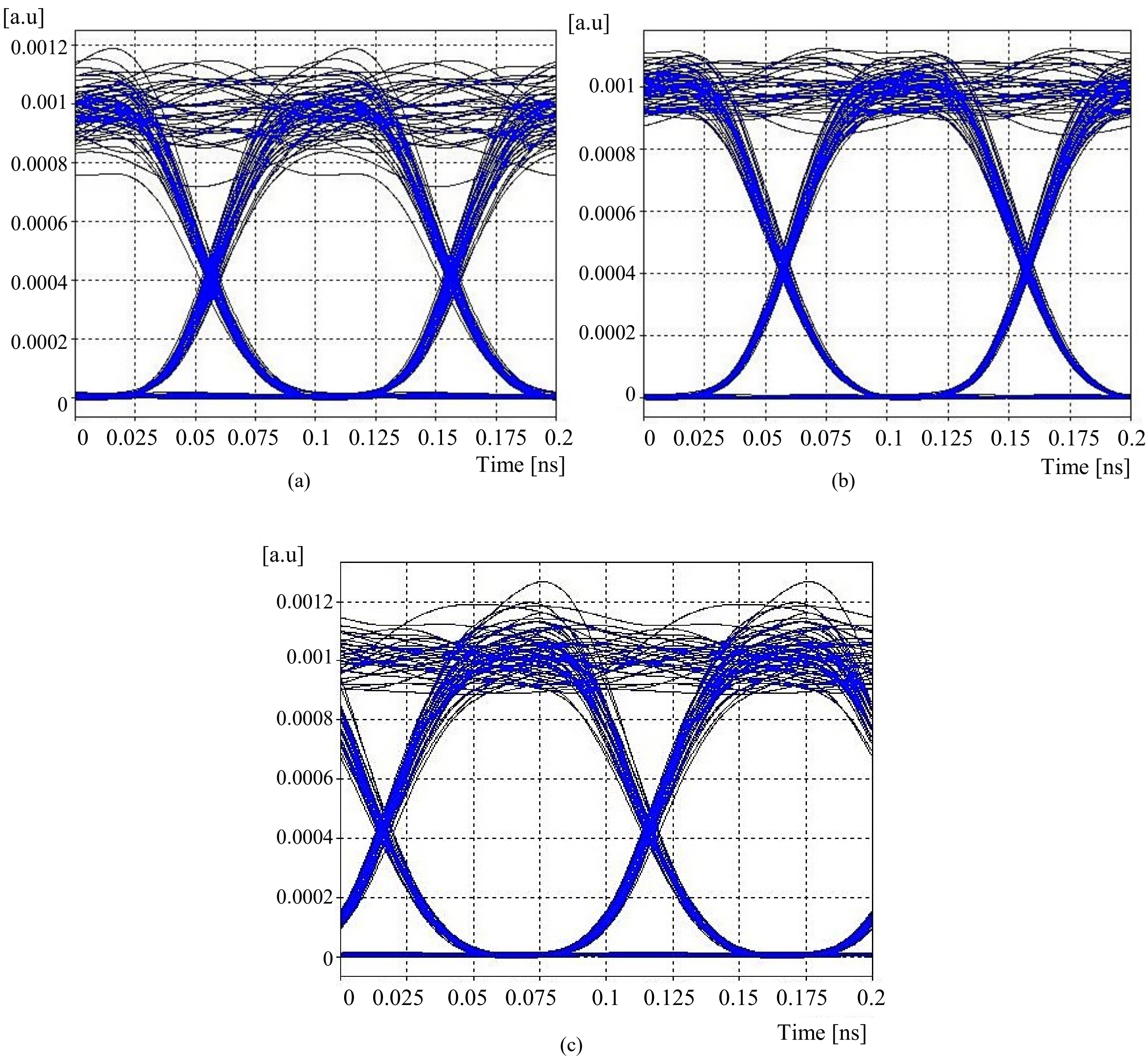

Fig. 8. Eye diagrams obtained for 32-channel TWDM/PON system using G-BP heterostructure based photodetector over 50 km for variable Doping concentration of BP layer (a) Low Doping (b) Moderate Doping (c) High Doping (colour online)

Fig. 8(a)-8(c) shows eye diagrams obtained for a 32-channel PON system using 1550 nm wavelength for variable doping concentrations of BP layer from low concentration to high concentration. Fig. 8(a) shows an eye diagram obtained for the proposed system using 1550 nm wavelength at a low doping concentration (~10^{12}). At low concentration of BP layer, the carrier density is low, hence magnitude of generated photocurrent is less. The quality of electrical output signal can be shown in the figure in the form of an eye diagram. The Q-factor is 21.68 dB, and the BER is 7.11×10^{-30}; these are the performance metrics achieved by this system at this concentration level.

Eye diagram for 32-channel PON system using 1550 nm wavelength at moderate doping concentration ($\sim 10^{12}$) is shown in Fig. 8(b). It is observed from the figure that the quality of received signal is improved at this concentration level. The carrier density increases at this level, resulting increase in photocurrent. The eye opening is maximum in this case among its counterparts. 25.3 dB is the maximum Q-factor attained by the system at this doping level of BP layer. In addition to this, the proposed system is simulated with a high doping ($\sim 10^{18}$) concentration of BP layer in G-BP heterostructure-based photodetector. The high doping level introduces noise in the detector during photo detection mechanism. Hence, the quality of the signal degrades at a higher doping level, as shown in the eye diagram. Fig. 8(c) shows the eye diagram obtained for the system at a higher doping concentration level of the BP layer. 22 dB is the Q-factor and 1×10^{-31} is the BER, achieved by the system at this concentration level. There are other performance metrics also, which decide the quantum efficiency of the photodetector. All the performance metrics are given in Table 1 and Table 2.

Table 1. Performance metrics of G-BP heterostructure-based photodetector at variable thickness of BP layer with constant moderate doping concentration of BP layer

BP Material Thickness	Q-factor	BER	Jitter	Eye-Closure
10 nm	22.9 dB	1×10^{-32}	0.022 ns	0.612 dB
25 nm	23 dB	1×10^{-34}	0.020 ns	0.588 dB
60 nm	25.3 dB	1×10^{-40}	0.018 ns	0.56 dB

Table 2. Performance metrics of G-BP heterostructure-based photodetector at variable doping level of BP layer with constant thickness (60 nm) of BP layer

BP Material Concentration	Q-factor	BER	Jitter	Eye-Closure
$N_{bp} = 1 \times 10^{12}$	21.68 dB	7.11×10^{-30}	0.023 ns	1.20 dB
$N_{bp} = 1 \times 10^{14}$	25.3 dB	1×10^{-40}	0.018 ns	0.56 dB
$N_{bp} = 1 \times 10^{18}$	22 dB	1×10^{-31}	0.021 ns	0.95 dB

All simulated results are obtained at channel-16 in the proposed network using G-BP heterostructure-based photodetector at ONU side. The effect of variation in thickness and doping level of BP layer has clearly shown in terms of eye diagrams obtained. Channel-16 is tuned to telecom operating wavelength, hence it is selected for all observations. Maximum Q-factor is attained at moderate doping concentration with 60 nm of thickness. The Q-factor of above 25 dB is attained by the system at a moderate doping concentration of BP layer with a higher thickness. Results confirm that doping concentration and thickness are the essential parameters for high-quality performance of the photodetector. 2D hybrid materials have a major effect in speeding up the photodetection mechanism performed by the photo detector. Research related to this field is continuously growing day by day. There is a comparison of some previous research work to the proposed work, which is presented in Table 3.

Table 3. Comparison of the previous research work with the proposed work

Parameters	Shuren Zhou et al. [15]	Shinpei Ogawa et al. [18]	Yanming Zhang et al. [22]	Xuemin Zhang et al. [23]	Proposed Work
Material used	Black-Si/Graphene	Graphene/Black phosphorus (G/BP)	Black phosphorus/Carbon nanotube (BP/C)	Graphene/Black phosphorus (G-BP)	Graphene/ Black phosphorus (G-BP)
Technique used/Performance metrics	The pyramidal device area is used to enhance responsivity	G/BP heterostructure-based metasurfaces	Strong electric field formation between black phosphorus (BP) and single-walled carbon nanotube (SWCNT)	Molybdenum is used as an electrode in G-BP heterostructure to reduce Schottky barrier	The efficiency of the photodetector is enhanced through the variable thickness and doping concentration of the BP layer.
Wavelength	Infrared	Infrared	1550 nm	637 nm	1550 nm
Work	In this work, ultrahigh responsivity, fast response, and broad spectral response are obtained for a wide range of applications. The graphene/Si van der Waals heterostructure offers a potential gain due to limited density of states near Dirac point. Pyramidal device area is used to enhance responsivity of the detector.	In this work, G/BP heterostructure-based metasurfaces are used to enhance the responsivity of the detector. The performance of BP metasurfaces is compared to the monolayer BP-based photodetector. The electron transfer in G/BP heterostructure-based photostructure is investigated theoretically. The absorption wavelength can be controlled by changing the thickness of G/BP strips. Results reveal that G/BP metasurfaces are considered as wavelength and polarisation-selective photodetectors.	High-performance photovoltaic infrared detectors and diodes are investigated on a BP/SWCNT-based photodetector. The external quantum efficiency of the detector is found to be maximum with carbon nanotubes. A strong electric field is formed between the junction of two materials. It favours energy band matching for the BP and SWCNT heterojunction. The strong ligh absorption and high carrier mobility enhance the responsivity and detectivity of the detector. About 0.52 A/W is the responsivity achieved by this heterojunction-based photodetector.	Realised a G-BP hetero structure-based photodetector for mid-wave infrared (MWIR) using molybdenum as an electrode to reduce the Schottky barrier. The device exhibits fast photo response within the range of 0.67 µm to 4.2 µm. A high photovoltaic responsivity up to 183 mA/W and external quantum efficiency (EQE) up to 35.6% are realised at the visible range of 0.637µm light. This work achieves rapid MWIR photo response at low light levels. The performance of a molybdenum-G-BP heterostructure is realised over a different wavelength.	In the proposed work, The opto-electronic properties of G-BP heterostructure-based photodetector are numerically investigated through COSMOL Multiphysics simulations. The performance of photodetector is investigated in a 32-channel high-speed TWDM/PON system using 1550 nm wavelength through eye diagrams obtained in OptSim simulations. A maximum Q-factor of 25.3 dB is attained at 60 nm thickness with moderate doping concentration of BP layer.

5. Conclusion

A 2D hybrid material including a G-BP heterostructure-based photodetector is successfully analysed in the proposed work. The standard dimensions are taken for the layered structure. The performance of G-BP heterostructure-based photodetector is investigated for variable wavelengths, doping concentration and thickness of BP layer. Maximum photoresponsivity is found to be 600 A/W over shorter wavelengths, such as 900 nm. At telecom operating wavelength (1550 nm), the photoresponsivity is slightly decreased. It can be enhanced with an increasing thickness of BP layer. On changing doping concentration of BP layer, the electric field formation at the junction gets affected. A moderate doping level is considered favourable for strong field formation. For further analysis, the photodetector is used in high speed optical network. 10 Gbps data is successfully transmitted in 32-channel high-speed TWDM/PON system using a 1550 nm wavelength with G-BP heterostructure-based photodetector at receiver terminal. The eye diagrams are obtained for variable thickness of BP layer, such as 10 nm, 25 nm, and 60 nm, keeping doping concentration constant. At 60 nm maximum Q-factor of 25.3 dB is attained by the system. To see the effect of doping concentration of BP layer, the system is simulated for low, moderate and high doping concentrations of BP layer. Moderate doping concentration gives the best result with a maximum Q-factor of 25.3 dB, keeping thickness constant of 60 nm, in comparison to its counterparts. Results reveal that high thickness and moderate doping level are suitable operating conditions for G-BP heterostructure-based photodetector over telecom operating wavelength ranges.

Acknowledgement

The authors express their appreciation to Guru Gobind Singh Indraprastha University (GGSIPU) for the continued facilitation provided via the Faculty Research Grant. The university's consistent patronage over the preceding years, including the current cycle, has been fundamental to the progression and maturation of this research. We value the institutional commitment to sustaining an environment conducive to longitudinal academic inquiry.

References

[1] N. Nandihalli, Critical Reviews in Solid State and Materials Sciences **49**(6), 999 (2024).
[2] M. W. Zulfiqar, S. Nisar, G. Dastgeer, M. Rabeel, H. Ghazanfar, A. Ali, M. Imran, H. Kim, D. K. Kim, Nanoscale **17**(31), 17881 (2025).
[3] M. Dai, X. Zhang, Q. J. Wang, Advanced Functional Materials **34**(21), 2312872 (2024).
[4] F. Zhong, H. Wang, Z. Wang, Y. Wang, T. He, P. Wu, M. Peng, H. Wang, T. Xu, F. Wang, J. Miao, W. Hu, Nano Research **14**(6), 1840 (2021).
[5] V. Sridhar, M. Rameez, P. Selvarasu, D. S. Tomar, S. Hegde, R. San Chen, C. T. Wu, C. H. Huang, S. Chattopadhyay, Materials Today Physics **40**, 101294 (2024).
[6] C. W. Jang, D. H. Shin, S. H. Choi, ACS Applied Electronic Materials **6**(8), 5517 (2024).
[7] A. Molaei-Yeznabad, K. Abedi, Scientific Reports **14**(1), 15291 (2024).
[8] H. Jiang, J. Wei, F. Sun, C. Nie, J. Fu, H. Shi, J. Sun, X. Wei, C. W. Qiu, ACS Nano **16**(3), 4458 (2022).
[9] L. Howe, K. H. Ellepola, N. Jahan, B. Talbert, J. Li, M. P. Cooney, N. Q. Vinh, ACS Applied Electronic Materials **7**(3), 1305 (2025).
[10] Y. Wang, V. X. Ho, Z. N. Henschel, P. Pradhan, L. Howe, M. P. Cooney, N. Q. Vinh, Infrared Sensors, Devices, and Applications X **11503**, 13 (2020).
[11] Q. Li, S. Fang, X. Yang, Z. Yang, Q. Li, W. Zhou, D. Ren, X. Sun, J. Lu, ACS Applied Materials & Interfaces **16**(46), 63786 (2024).
[12] F. Wang, H. Xu, Q. Gu, C. Shi, L. Zhang, Z. Wu, G. Deng, H. Zhou, A. T. S. Wee, S. Zhou, Optics Letters **50**(12), 4098 (2025).
[13] R. K. Mishra, J. Sarkar, I. Chianella, S. Goel, H. Y. Nezhad, Next Materials **4**, 100217 (2024).
[14] L. Cui, M. Sun, The Journal of Physical Chemistry C **125**(40), 22370 (2021).
[15] S. Zhou, H. Fan, S. Wen, R. Zhang, Y. Yin, C. Lan, C. Li, Y. Liu, Advanced Optical Materials **12**(9), 2301982 (2024).
[16] R. Li, M. Wang, H. Xing, M. Sun, H. Xie, W. Qiu, Acta Mechanica Solida Sinica **38**(2), 309 (2025).
[17] W. Yang, J. Chen, Y. Zhang, Y. Zhang, J. H. He, X. Fang, Advanced Functional Materials **29**(18), 1808182 (2019).
[18] S. Ogawa, S. Fukushima, M. Shimatani, M. Iwakawa, Journal of Applied Physics **136**(19), 193101 (2024).
[19] F. Yan, C. Hu, Z. Wang, H. Lin, K. Wang, Applied Physics Letters **118**(19), 190501 (2021).
[20] R. Liu, F. Wang, L. Liu, X. He, J. Chen, Y. Li, T. Zhai, Small Structures **2**(3), 2000136 (2021).
[21] C. R. Ryder, J. D. Wood, S. A. Wells, M. C. Hersam, ACS Nano **10**(4), 3900 (2016).
[22] Y. Zhang, Q. Li, X. Ye, L. Wang, Z. He, T. Zhang, K. Wang, F. Shi, J. Yang, S. Jiang, X. Wang, C. Chen, Nanomaterials **13**(19), 2700 (2023).
[23] X. Zhang, C. Yan, X. Hu, Q. Dong, Z. Liu, W. Lv, C. Zeng, R. Su, Y. Wang, T. Sun, Z. Xing, C. Pang, B. Zhang, W. Shi, M. Long, Materials Research Express **8**(3), 035602 (2021).
[24] A. Patra, M. A. More, D. J. Late, C. S. Rout, Journal of Materials Chemistry C **9**(34), 11059 (2021).
[25] S. Vankalayapati, Y. Vasimalla, A. Katakamsetty, J. Vaadaala, B. Ramachandran, C. Santhosh, S. Maloji, S. Kumar, Plasmonics **20**(7), 5215 (2025).
[26] H. Bouandas, Y. Slimani, A. Bakhouche, N. Bioud, A. Djemli, F. K. Alanazi, I. Bouchama, M. A. Ghebouli, M. Fatmi, T. Chihi, Results in Physics **66**, 108004 (2024).
[27] W. Zhang, F. Qiu, Y. Li, R. Zhang, H. Liu, L. Li,

J. Xie, W. Hu, ACS Nano **15**(8), 13370 (2021).

[28] Z. Qi, L. Li, Z. P. Xu, Particuology **64**, 121 (2022).

[29] W. Ahmad, J. Kazmi, M. Z. Nawaz, A. E. Moutaouakil, J. Zhang, Y. Illarionov, Z. Wang, Advanced Functional Materials **36**(24), e16893 (2025).

[30] N. A. N. Phan, H. Noh, J. Kim, Y. Kim, H. Kim, D. Whang, N. Aoki, K. Watanabe, T. Taniguchi, G. H. Kim, Small **18**(13), 2105753 (2022).

[31] F. Zhou, Heliyon **10**(14), e34684 (2024).

[32] A. Abderrahmane, C. Woo, P. J. Ko, Journal of Electronic Materials **50**(10), 5713 (2021).

[33] C. Liu, S. Ding, Q. Tian, X. Hong, W. Su, L. Tang, L. Wang, M. Zhang, X. Liu, Y. Lv, J. C. Ho, L. Liao, X. Zou, Laser & Photonics Reviews **17**(2), 2200486 (2023).

[34] Y. Zhou, H. Qiao, Z. Huang, Q. Ma, F. Liu, G. Liao, S. Luo, J. Zhong, X. Qi, ACS Sustainable Chemistry & Engineering **9**(44), 14918 (2021).

[35] H. Zhang, R. A. A. Osama, R. Cheung, Computational Condensed Matter **44**, e01071 (2025).

[36] Y. Chen, Y. Zhang, K. Cai, J. Jiang, J. C. Zheng, J. Zhao, N. Wei, Carbon **117**, 399 (2017).

[37] X. G. Ye, Z. T. Zhang, P. F. Zhu, W. Z. Xu, A. Q. Wang, Z. M. Liao, Physical Review B **111**(4), L041403 (2025).

[38] X. Fu, X. Cheng, D. Wu, W. Liao, J. Guo, B. Bao, L. Li, Superlattices and Microstructures **160**, 107084 (2021).

[39] L. Wu, J. Guo, Q. Wang, S. Lu, X. Dai, Y. Xiang, D. Fan, Sensors and Actuators B: Chemical **249**, 542 (2017).

[40] S. Thurakkal, D. Feldstein, R. Perea-Causín, E. Malic, X. Zhang, Advanced Materials **33**(3), 2005254 (2021).

*Corresponding author: ckumarggsipu@gmail.com